Applications of cyclotron based ion scattering

Nuclear Instruments and Methods in Physics Research B 89 (1994) 114–121
North-Holland

NIM B
Beam Interactions with Materials & Atoms

Applications of cyclotron based ion scattering

L.J. van IJzendoorn, J.W. Niemantsverdriet, R.J. Severens, P.W.L. van Dijk, M.J.A. de Voigt
Cyclotron Laboratory, Physics Department, Eindhoven University of Technology, and Schuit Institute of Catalysis, P.O. Box 513, 5600 MB Eindhoven, The Netherlands

Ion scattering experiments have been performed with a 3–30 MeV AVF cyclotron. The wide range of available energies combined with proper beam handling allows many scattering techniques to perform. At first an example of ordinary Rutherford backscattering spectrometry will be demonstrated on model catalysts as studied in surface chemistry. High energy backscattering spectrometry with 8.8 MeV He ions, which enhances the sensitivity for oxygen, has been applied to study the oxygen removal from corroded archaeological artefacts upon treatment with a H_2 plasma. Elastic recoil detection analysis will be shown feasible with He ions having incident energies between 10 and 15 MeV once combined with a thin film detector. The development of a setup for ion channeling experiments with the cyclotron is reported and first results promise to increase the angular resolution in lattice deformation studies.

1. Introduction

Cyclotrons have been used for exploring nuclear structure for more than 50 years. With the ever increasing demand for higher particle energies in nuclear physics on one hand and the demand for socially relevant applications of cyclotrons on the other hand, the low energy cyclotrons become available for materials science studies and other applications.

Reported applications of cyclotrons in materials science can be found in the areas of radiation damage studies, materials modification studies and applications in analysis techniques. Independently, the production of radioisotopes is well established [1,2]. The production of γ-emitters like ^{111}In, ^{67}Ga and ^{123}I are widely applied in nuclear medicine and the production requires proton energies up to 30 MeV. Short lived positron emitters such as ^{11}C, ^{13}N and ^{15}O can be produced with proton energies up to ~16 MeV and are incorporated in radiochemicals for applications with positron emission tomography (PET) in nuclear medicine. Positron emitters and PET have also been used recently in the investigations of reaction kinetics of car exhaust catalysts [3].

The surplus value of the available high energy ion beams for radiation damage studies mostly concerns investigations on wall materials in nuclear reactors and materials applied in satelites. For the latter, both the failure of electronic devices upon radiation with e.g. 60 MeV protons and even many heavy ions at energies up to 500 MeV [4,5] as well as the decrease in optical transparancy in glasses [4] is subject of investigation. Materials modification is usually carried out with heavy ion beams at several hundreds of MeV exploring the properties of long range columnar defects in materials. At present, probably the most well known examples are the enhancement of the critical current in high-T_c-superconductors (e.g. 500 MeV ^{129}I ions in $Bi_2Ca_{n-1}Sr_2Cu_nO_{2n+4-\delta}$ [6] and 580 MeV ^{116}Sn ions in $Y_1Ba_2Cu_3O_{7-\delta}$ [7]), and the production of micro filters with pore dimensions in the order of several microns [8].

Application of cyclotron beams for analysis purposes has been biased towards charge particle activation analysis (CPAA) and in particular thin layer activation (TLA). An important application area is mechanical engineering, in particular wear studies on engines [9] using many different radioisotopes. The use of cyclotrons for ion scattering studies is rare due to competition from small Van de Graaff and tandem accelerators. Instrumental difficulties are the relatively low brightness of the accelerator which is typically a factor of 10–100 below reported brightnesses for Van de Graaff accelerators (reported as high as 5 $\mu A/mm^2$ $mrad^2$ [10]) and the energy spread of $\Delta E/E \approx 3 \times 10^{-3}$ mostly due to phase differences between orbits and multiturn extraction. However, the energy resolution in ion scattering experiments can be improved by using dispersive magnets and slits in the beam guiding system which lowers the energy spread by a factor of 5–10: $\Delta E/E \sim 5 \times 10^{-4}$. This energy spread (e.g. 5 keV for 9 MeV αs) is below the typical energy resolution of a surface barrier detector normally used in ion scattering analysis techniques and does not impose serious re-

SSDI 0168-583X(93)E0767-B

strictions. Furthermore, a very broad energy regime is at hand in particular for protons and α-particles which is out of reach for the smaller accelerators.

At Eindhoven University of Technology (EUT) an effort is undertaken to apply a 3–30 MeV AVF Cyclotron (AVF: azimuthally varying field) in ion scattering experiments for materials science and surface chemistry and to explore scattering at high beam energies. The present paper will report on several applications and developments.

The first application shows ordinary Rutherford Backscattering Spectrometry (RBS) with 4 MeV He^+ particles applied in surface chemistry (catalysis). Next, high energy backscattering spectrometry (HE-BS) with 8.8 MeV α-particles was applied to study the reduction of iron oxides with a hydrogen plasma for the conservation of archeological artefacts. The availability of 10–15 MeV He^{2+} beams stimulated us to develop high energy recoil spectrometry (HE-RS) which turns out to be an interesting alternative for the use of heavy ion beams in ERDA. Finally, another specific merit of cyclotron based ion scattering will be the application of channeling at high beam energies which promises to reach unprecedented angular accuracies for lattice deformation studies with ion beams.

2. RBS in catalysis

The application of surface analysis techniques in catalysis is practically limited by the powder form of the high surface area supports. Electron or ion spectroscopies suffer from sample charging of the rough and insulating surface. During the last decade several authors [11–13] circumvented these problems by using model supports consisting of flat silicon or aluminium crystals with a thin (natural) oxyde layer of a few nanometers on top. The active metals were usually deposited on the substrate by evaporation or by decomposition of suitable metal carbonyls. The essential steps in the preparation of commercial powder catalysts are however wet chemical deposition followed by drying, calcination and reduction of the active metals. At the chemistry department of EUT this procedure is applied on model catalysts and the intermediate products are analysed with surface spectroscopies to understand and optimize the preparation procedure [14–16]. X-ray photoelectron spectroscopy (XPS) is applied to obtain the oxidation state of the metals, static secondary ion mass spectrometry (SSIMS) is used to investigate the local environment and atomic force microscopy to study surface morphology. RBS contributes significantly in quantifying the surface coverage and obtaining possibly depth profiles. The cyclotron is typically operated to produce 4 MeV He^+ particles with an energy spread of 9 keV ($\Delta E/E \sim 2 \times 10^{-3}$) with typically 100–200 nA beam current at 1–2 mm^2 resulting in an overall system resolution of 18 keV. Applying RBS at this energy requires careful use of Rutherford cross-sections. Bozoian [17] developed a model to estimate the energy where 4% deviation to Rutherford cross-sections occurs which results for $^{28}Si(\alpha, \alpha)^{28}Si$ at 170° laboratory backscattering angle in 3.95 MeV. For the catalytic metals like Rh, Pt, Zr, Mo sited on top of the Si or Al substrate, Rutherford cross-sections are appropriate. An example concers the preparation of a $Rh/Al_2O_3/Al$ model catalyst. Rh on alumina is essential in automotive car exhaust catalysis because of its high selectivity in the reduction of NO_x (see e.g. ref. [18]) through $2NO + 2H_2 \rightarrow N_2 + 2H_2O$ under slightly reducing conditions. This catalyst is prepared by impregnating the Al_2O_3 support with an aqueous solution containing $RhCl_3$. In water, the Rh^{3+} ion is surrounded by six ligands which can be Cl^-, OH^- and H_2O represented by $[RhCl_x(H_2O)_y(OH)_z]^{n-}$. Negatively charged complexes adsorb as the result of an electrostatic interaction with positively charged sites on the alumina surface, while neutral complexes might attack to the support through a reaction with surface OH groups [19]. The pH of the impregnating solution is of crucial importance in the preparation of the catalyst. The pH of the solution must be well below the iso-electric point of alumina (pH ≈ 7) in order to create a positive charged surface while on the other hand the pH should not be too low to prevent dissolution of the Al_2O_3. Dissolved alumina will react with Rh complexes and precipitate in an uncontrolled way during drying. Fig. 1 shows RBS spectra in the region near the Rh surface peak of impregnated Al_2O_3/Al model catalysts with solutions having pH values ranging from 2

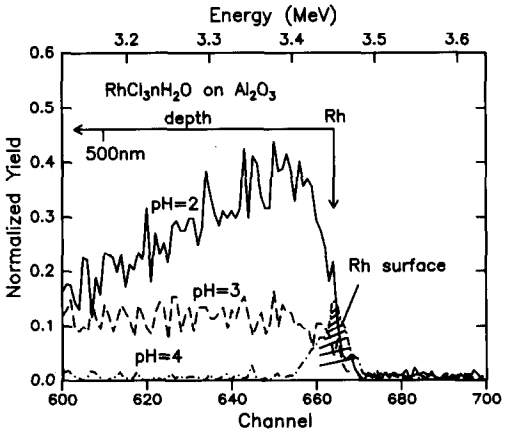

Fig. 1. RBS spectra near the Rh surface position of impregnated Al_2O_3/Al model supports. The spectra have been measured with 4 MeV He^+ ions incoming along the surface normal and a scattering angle of 165°.

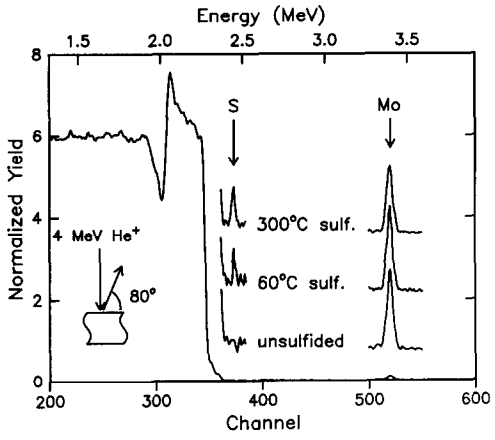

Fig. 2. RBS spectra showing the sulfidation of a $MoO_3/SiO_2/Si$ model catalyst. The spectra were measured with 4 MeV He^+ ions incoming at an angle of 5° with respect to the surface normal and a scattering angle of 170°.

to 4. The Rh depth profiles for pH = 2 and 3 clearly indicate the precipitation of Rh particulates while a pH = 4 results in a Rh loading at the surface equal to 1.1×10^{15} at/cm^2. The occurence of acid attack can also be measured with XPS which shows a decreased Al^{3+}/Al intensity ratio when pH < 4 [19].

A second example concerns the study of molybdenumsulfide catalysts on a $SiO_2/Si(100)$ model support. MoS_x catalysts are used for the hydrodesulfurisation (HDS) or hydrodenitrogenation (HDN) of heavy oil fractions [20]. In the laboratory, these catalysts are prepared by dissolving MoO_2Cl_2 in ethanol and wetting (impregnating) the support using the spincoating technique. Subsequently the samples are dried and sulfided in H_2S/H_2 at temperatures between 100 and 300°C. Understanding the sulfidation mechanism is important to prepare the correct MoS_{2-x} catalyst and was extensively studied by so-called temperature programmed sulfidation in which the gasses consumed or produced in a sulfidation reactor (H_2S, H_2O and H_2) were analyzed (see e.g. ref. [21]). The application of XPS, SIMS, AFM and RBS on model catalysts however enables to establish the stable phases in the catalyst after the subsequent phases of the sulfidation treatment. Fig. 2 shows the RBS spectra taken with 4 MeV He^+ ions of $MoO_xS_y/SiO_2/Si(100)$ model catalysts directly after preparation and after subsequent sulfidation at 60°C and 300°C. The areal densities of Mo and S have been calculated using Rutherford cross-sections; the threshold for non-Rutherford scattering at 170° laboratory scattering angle is 4.5 MeV for S. The S/Mo ratio calculated from the RBS spectra was found between 1 and 1.5 for catalysts sulfided at room temperature and at 60°C but increased to values between 2 and 2.5 when the sulfidation temperature is 100°C or higher.

Important is the observation with atomic force microscopy that the impregnation process resulted in disk shaped particles with a diameter $\lesssim 100$ nm and at most 5–10 nm thick. The specific surface sensitive spectroscopies as XPS and SSIMS could be combined with the RBS data to obtain a measure of the sulfur gradient from the outside of the particles to the "bulk" by evaluating the quotient of the S/Mo ratio from RBS with the S/Mo intensity ratio from XPS. XPS studies on the Mo(3d) and S(2p) binding energies indicated the coversion of Mo^{6+} to Mo^{4+} upon sulfidation at room temperature and provided evidence for the presence of an S_2^{2-} intermediate at sulfidation temperatures below 150°C SSIMS proved the presence of MoO_xS_y intermediates at sulfidation temperatures of 25 and 60°C. The combined information allowed to unravel the detailed sulfidation mechanism of MoO_3 to MoS_2 through MoO_xS_y intermediates [16].

The two examples above show that RBS can serve as a useful supplement to surface spectroscopies in the analysis of model catalysts.

3. HE-BS for conservation of archaeological artefacts

The use of HE-BS with 8.8 MeV He ions is well established for the analysis of oxygen in high temperature superconductors [22]. At EUT this technique has been applied to obtain the oxygen concentration in corroded iron arehaeological artefacts which have been conserved with a hydrogen plasma.

For conservation of archaeological excavations it is necessary to stop the corrosion process. Corrosion is the result of an electrochemical reaction which oxidizes Fe to Fe^{2+} and/or Fe^{3+} at anodic spots at the surface of the artefact and reduces oxygen by $O_2 + 2H_2O + 4e \rightarrow 4OH^-$ at cathodic spots. In a high chloride content environment such as sea water, Cl^- is catalyzing the reaction due to enhanced ionic conduction in the solution and β-FeOOH, Cl_x with $x \lesssim 0.05$ or lepidocrocite: γ-8FeOOH,FeOCl are formed as precipitates. After excavation, hygroscopic chlorides cause an aqueous phase to exist at only 20% relative humidity and acid containing pits accelerate the corrosion process due to the virtually unlimited supply of oxygen through air. Conservation of archaeological artefacts thus implies removal of the chlorides and if possible the removal of the oxidized crust.

Most of the removal techniques are based on wet chemistry (see e.g. the alkaline sulphite treatment [23]). These methods are time consuming (typically months of reaction time) laborious and not always succesful. In 1979 Daniels [24] used a low temperature hydrogen glow discharge for cleaning silver artefacts and later

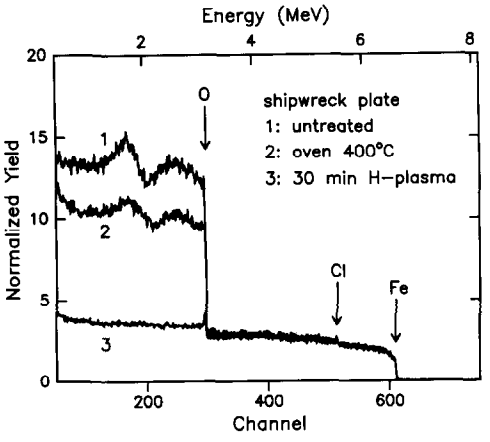

Fig. 3. HE-BS spectra measured with 8.8 MeV He^{2+} ions at normal incidence. The scattering angle adopted was 165°. The spectra have been normalized on the Fe stepheight demonstrating the oxygen removal from the corroded specimen.

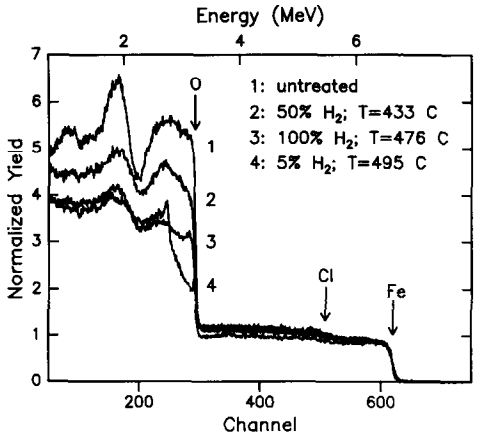

Fig. 4. HE-BS spectra demonstrating the removal of oxygen under varying conditions in an Ar/H_2 plasma. The measuring conditions are as in Fig. 3.

Vepřek and coworkers extended the method using an RF glow discharge [25]. The hydrogen plasma reduces the oxidized crust on the timescale of minutes and the remainder can be easily removed with a scalpel. At EUT cleaning with a cascaded arc plasma source is investigated [26]. The source can be placed outside an expansion chamber thus avoiding coupling of the RF field with heavy iron artefacts. The ongoing reduction process was investigated with HE-BS while the removal of chlorine was measured with proton induced X-ray emission using 3 MeV H^+ ions.

Fig. 3 shows three HE-BS spectra of a shipwreck plate, the first spectrum is of the untreated specimen, spectrum no 2 after heating in a vacuum oven at 400°C during 30 min and spectrum no 3 after 30 min in a plasma obtained from an $Ar/H_2 = 3/1$ gas mixture. The spectra in Fig. 3 are normalized on the Fe stepheight thereby elucidating the oxygen removal. The threshold for non-Rutherford scattering of He ions on Fe at a backscattering angle of 165° is ~ 6.9 MeV [17] and therefore the ratio of the cross-section for scattering of He on O and Fe was measured using a bulk single crystalline Fe_3O_4 sample. The untreated shipwreck plate exhibits an atomic O/Fe ratio of 2.3 ± 0.15, in agreement with the expected FeOOH phase. Heating in the vacuum oven results in dehydratation through: $2FeOOH \rightarrow Fe_2O_3 + H_2O\uparrow$ as concluded from the measured O/Fe-ratio of 1.5 ± 0.1 in the second spectrum. The hydrogen plasma facilitates almost complete reduction of the ironoxydes: $O/Fe = 0.1 \pm 0.03$.

In order to gain some insight in the reduction process, a set of experiments on heavily corroded steel plates has been performed varying the Ar/H_2 ratio of the incoming gas. Fig. 4 shows several HE-BS spectra after 10 min in the plasma expansion chamber. Apparently, the Ar/H_2 gas ratio is not the dominating parameter, instead a strong correlation with sample temperature during the treatment was found as depicted in Fig. 5. The vertical scale in Fig. 5 gives the oxygen concentration in the first μm normalized on the untreated specimen. Obviously, treatment with an Ar plasma or heating in an oven only dehydrates the ironoxyde layer and hydrogen in the plasma is required to reduce the oxydes. At present, the complicated interplay between dehydration and reduction during plasma bombardment of the (hydrated) corroded layer

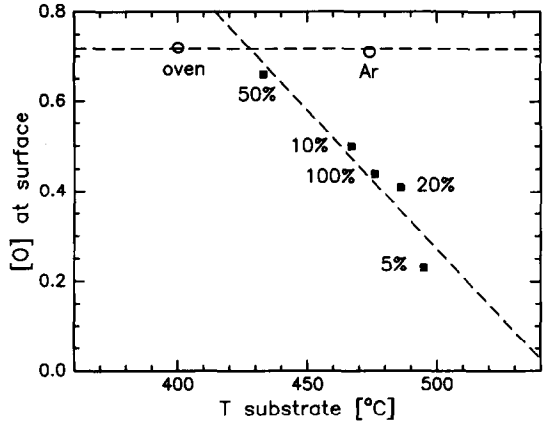

Fig. 5. Oxygen concentrations as measured with HE-BS near the surface of conserved Fe archaeological artefacts. The hydrogen volume fraction of the incoming gas is indicated: $n\%$ corresponds to $n\%$ H_2 and $(100-n)\%$ Ar. The indication "Ar" represent an Ar plasma without the addition of hydrogen and "oven" represents annealing in vacuum. The dashed lines are not based on a model but only shown to elucidate the difference between dehydration and reduction.

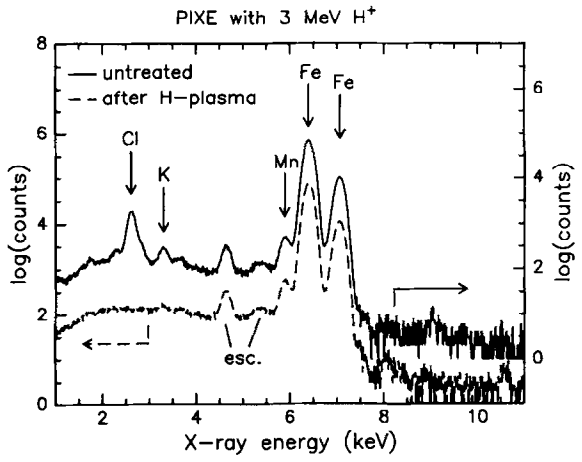

Fig. 6. PIXE with 3 MeV H^+ demonstrating the removal of Cl in an $Ar/H_2 = 9/1$ plasma during 20 min. The atomic Cl concentration drops from 5% in the untreated specimen to less than 100 ppm after plasma bombardment. The two Fe peaks correspond to the $Fe-K_\alpha$ at 6.399 keV and the $Fe-K_\beta$ at 7.059 keV. The Fe escape peaks shifted by 1.75 keV ($Si-K_\alpha$) are indicated.

prevents to draw unambigious conclusions on the reaction mechanism. A set of experiments on dehydrated corroded layers is presently in progress.

Fig. 4 also shows the changing morphology by the spreading of the oxygen resonance structure. This can be attributed to cracks in the sample (allowing the easy removal of the crust) which result in varying pathlengths of the scattered He ions along the outgoing path. Although the removal of Cl can be observed in Fig. 4, PIXE measurements as shown in Fig. 6 show the removal of Cl much more clearly. Although a reduction of Cl content by 85% in the oven and 99.5% in an Ar plasma was measured, complete chlorine removal below the detection limit of PIXE (100 ppm) is only found in H_2 containing plasmas which allow the removal of Cl included in the oxyde matrix.

4. ERDA with high energy α-beams

Elastic Recoil Detection is a well established ion beam analysis technique to profile light elements such as C, N and O in thin films up to 100 nm [27]. For the detection of light elements on heavy substrates, typically ^{35}Cl or ^{28}Si beams with energies around 30 MeV are used as incident beams. A cyclotron allows the use of He beams with energies above 10 MeV which can also be applied to recoil light elements out of a specimen. In this respect it should be noted that the kinematic factor, giving the fraction of beam energy transferred to the recoils, only depends on μ (μ represents the ratio of projectile mass M_1 and the mass of the recoiled target nucleus M_2) and the recoil angle ϕ and does not change when μ is replaced by $1/\mu$. This means that approximately the same fraction of beam energy is transferred to a carbon recoil by a He ion as by a Cl ion. This implies that 10–15 MeV He beams and recoil angles between 30° and 45° produce C, O and N recoils with kinetic energies between ~3 and 8 MeV. In this energy regime the electronic stopping power of these recoils reaches its maximum thus facilitating easily depth resolutions on the order of 10–15 nm near the surface. The experimental problem to overcome is the large flux of forwardly scattered projectiles in the direction of the detector. Instead of using a stopper foil in combination with a standard surface barrier detector, as is usually employed for heavy incident ions, in the present case detectors with thin depletion zones should be applied. The experiment has to be designed such that the projected range of the recoils is slightly less than the thickness of the depletion layer. The scattered particles will pass through and deposit only a limited amount of energy by electronic stopping. This setup can be realized by either thin film detectors [28] or the use of pulse shape discrimination techniques [29] in low resistive PIPS detectors using low bias voltages and thus thin depletion zones.

Merits of high energy low mass projectiles are twofold: the radiation damage to samples is low and a larger probing depth than in conventional ERDA can be reached. The omission of a stopper foil causes no additional energy straggling of the detected recoils after departure from the samples which basically enhances the depth resolution. Unfortunately this advantage is perished by the "virtual absence" of stopping of the incoming He ions which in turn decreases the depth resolution. The net depth resolution is comparable to conventional ERDA with heavy ion beams.

A more serious problem encountered when using high energy alpha beams concerns the elastic scattering cross-sections. The incident energy is far beyond the threshold for non-Rutherford scattering and also inelastic scattering may occur. Energy spectra of scattered α-particles with incident energies in the range up to 20 MeV have been used extensively in nuclear physics. Usually, excitation spectra at a few well defined scattering angles were measured. Unfortunately these scattering angles are different for each specific atom. In order to apply nuclear scattering or the related recoil detection in materials analysis, the cross-sections for several inelastic and elastic scattering processes of a number of atoms e.g. C, N and O, have to be known at the same particular recoil angle and incident energy. A set of experiments has been performed to obtain the angle dependent cross-sections for C, O and N at 11.9, 13.4 and 14.6 MeV [28]. These energies have been chosen to reach maximum cross-

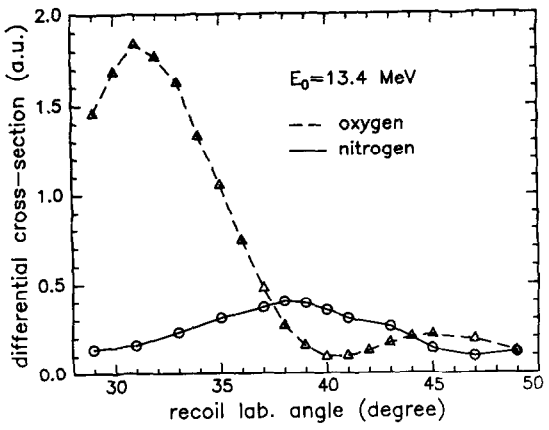

Fig. 7. Measured angle dependent differential recoil cross sections for O and N with 13.4 MeV He ions. The drawn lines are not based on a model but only to guide the eye. The size of the error bars is approximately equal to the size of the symbols and are ommitted for clarity.

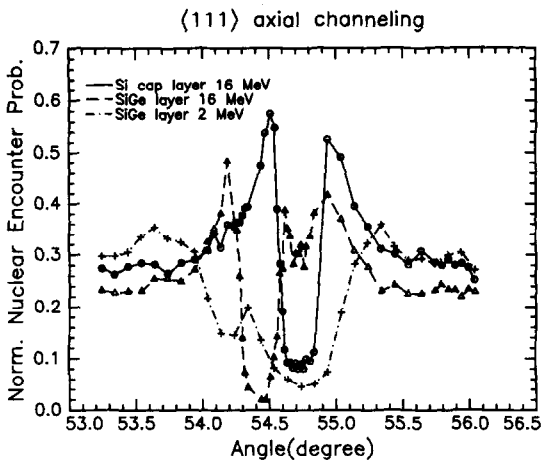

Fig. 9. Calculated angular scans from Monte Carlo trajectory calculations of a 50 nm Si/50 nm $Si_{0.83}Ge_{0.17}$/Si(100) using 2 and 16 MeV He ions. The drawn lines are only to guide the eye.

sections for recoiling C, O and N respectively. Typical values are in the range 50–200 mb/sr. Fig. 7 shows results on the angle dependent cross-sections for oxygen and nitrogen using 13.4 MeV He ions. The interesting possibility occurs to alter the relative sensitivities for O and N by changing the recoil angle from 30 to 40 degrees. Although 13.4 MeV is chosen to reach maximum sensitivity for oxygen, changing the recoil angle allows quick inspection for the presence of nitrogen. An example of the recoil spectra obtained is depicted in Fig. 8 which shows the oxygen profile in a $SiO_{1.5}N_{0.34}$ layer on Si. Currently HE-ERDA is applied in the analysis of the composition of various plasma deposited coatings such as α-Si: H, α-C layers and $B_xN_yC_z$ wear resistant layers.

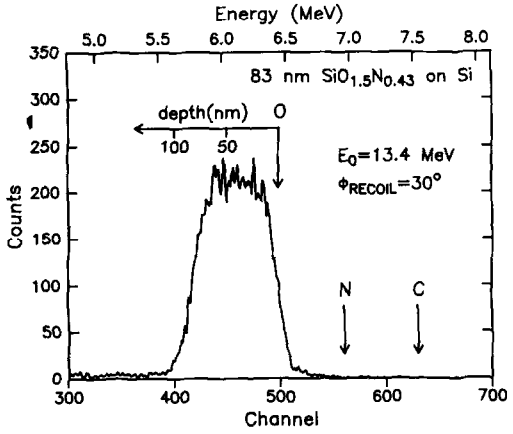

Fig. 8. ERDA spectrum measured with a 5 μm thick surface barrier detector. The energies of elastically recoiled C, N and O from the surface are indicated by the arrows. The angle between the incoming beam and the sample normal was 15°.

5. Channeling with high energy protons or α-particles

One of the applications of ion channeling is the analysis of lattice deformation e.g. strain in epitaxial layered systems. The parameter decisive for the ultimate angular resolution is the critical angle for channeling ψ_c [30]. Both for planar and axial channeling, ψ_c is proportional to $(Z_1Z_2/E)^{1/2}$. Z_1 is the charge of the projectile, Z_2 the charge of the target nucleus and E the energy of the incoming particles. This proportionality implies that high energy α or proton beams from a cyclotron promise to reach enhanced angular resolutions. An example of the possible merit of this effect is illustrated in Fig. 9. This figure contains calculated angular scans through the ⟨111⟩ axial minimum in the ⟨110⟩ plane of a 50 nm Si/50 nm $Si_{0.83}Ge_{0.17}$/Si(100) layered structure. The calculations have been performed for beam energies of 2 and 16 MeV with the Monte Carlo code LAROSE [31,32]. The tetragonal deformation of the SiGe layer shows up in the simulations with 2 MeV He ions as a double peak structure. Apparantly a substantial amount of the ions channeled in the Si capping layer arrives within the critical acceptance angle of the SiGe layer at the Si/SiGe interface and thus produces a minimum around 54.7° and results in a double minimum in the yield. Increasing the energy up to 16 MeV results in narrow angular scans and small values of ψ_c. Note that the minimum corresponding to channeling in the SiGe layer shifts as a function of energy. This effect illustrates the depth

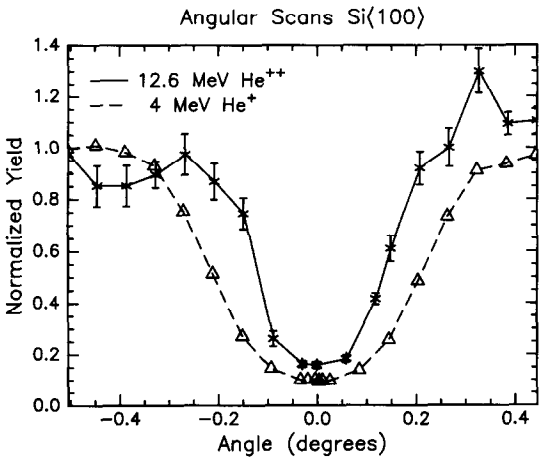

Fig. 10. Measured angular scans through the axial Si⟨100⟩ minimum with 4 MeV and 12.6 MeV He ions from a cyclotron. The drawn lines are to guide the eye.

dependence of the mean angular direction of the channeled beam. As a result, beam steering is strongly reduced and the resulting angular resolution is enhanced by a factor of ~3. Obviously further increase of the beam energy and the use of protons will improve the angular resolution further.

In order to realize these experiments two instrumental problems have to be overcome. At first a goniometer has to be obtained with an angular accuracy of ~0.005°. At EUT such a goniometer was build in close coorporation with the faculty of mechanical engineering. The three axis goniometer is UHV compatible, has motors outside the vacuum and allows also transmission experiments to be carried out. A detailed description and test results on the angular accuracies will be published in the near future. The second problem concerns the relative low brightness of the cyclotron which hampers high beam currents at small angular divergencies. We nevertheless succeeded to obtain a ~60 nA beam current with an angular divergence of 0.04° with 12.6 MeV He^{2+} ions on an area of several mm^2. Fig. 10 shows two measured angular scans through the Si⟨100⟩ axial minimum using 4 and 12.6 MeV He ions respectively. The angular scan at 4 MeV was recorded with a scattering angle of 145° and 90″ acquisition time per data point. The scan recorded at 12.6 MeV was measured with a scattering angle of 135° and 180″ data-acquisition time per data point. In both cases the scattering yield was integrated over a depth interval of 1.1 μm. The reduction in Ψ_c is clearly observed and experiments on strained InGaAs/InP layers are currently in progress to investigate the experimental angular accuracies which can be reached.

6. Conclusions

It has been demonstrated that a cyclotron can be succesfully applied in ion scattering experiments. Ordinary RBS can be performed while in addition the high beam energies offered by the cyclotron facilitates the use of HE-BS which allows to enhance the sensitivities for light elements at specific incident energies and scattering angles. High energy recoil spectrometry (HE-RS) with 10–15 MeV α-beams appears an interesting alternative for conventional ERDA with heavy ion beams offering low radiation damage and larger probing depth. Channeling experiments with high energy α or proton beams have been shown feasable and offer an enhanced angular resolution in lattice deformation studies. The application of RBS in the area of surface chemistry has been demonstrated by the analysis of model catalysts. HE-BS was shown to be a valuable tool for the analysis of iron oxydes which is of relevance for conservation of archaeological excavations.

References

[1] H.N. Wagner Jr., J. Nucl. Med. 27 (1986) 1929.
[2] D.J. Silvester, in: Proc. 7th Int. Conf. on Cyclotrons and their applications (Birkhäuser, Basel, 1975) p. 408.
[3] G. Jonkers, K.A. Vonkeman, S.W.A. van der Wal and R. van Santen, Nature 355 (1991) 63.
[4] K. Ziegler, in: Proc. of 13th Int. Conf. on Cyclotrons and their applications (World Scientific, Singapore, 1991) p. 151.
[5] A.B. Campbell, W.J. Stapor, K. Koga and W.A. Kolasinski, IEEE Trans. Nucl. Sci. NS-32 (1985) 4150.
[6] L. Civale, A.D. Marrick, T.K. Worthington, M.A. Kirk, J.R. Thompson, L. Krusin-Elbaum, Y. Sun, J.R. Clem and F. Holzberg, Phys. Rev. Lett. 67 (1991) 648.
[7] W. Gerhäuser, G. Ries, H.W. Neumüller, W. Schmidt, O. Eibl, G. Saemann-Ischenko and S. Klaumünzer, Phys. Rev. Lett. 68 (1992) 879.
[8] B.E. Fischer and R. Spohr, in: Proc. of 12th Int. Conf. on Cyclotrons and their Application (World Scientific, Singapore, 1991) p. 555.
[9] D.P. Chowdury, J. Chaudhuri, V.S. Raju, S.K. Das, B.B. Bhattacharjee and S. Gangadharan, Nucl. Instr. and Meth. B 42 (1989) 375;
A. Gervé and G. Schatz, in: Proc. 7th Int. Conf. on Cyclotrons and their applications (Birkhäuser, Basel, 1975) p. 496.
[10] D.N. Jamieson, G.W. Grime and F. Watt, Nucl. Instr. and Meth. B 40/41 (1989) 669.
[11] L.H. Dubois, P.K. Hansma and G.A. Somorjai, Appl. Surf. Sci. 6 (1980) 173.
[12] J.G. Chen, M.L. Colaianni, P.J. Chen, F.T. Yates and G.B. Fisher, J. Phys. Chem. 94 (1990) 5059.
[13] D.N. Belton and S.J. Schmieg, Surf. Sci. 199 (1988) 518.
[14] L.M. Eshelman, A.M. de Jong and J.W. Niemantsverdriet, Catal. Lett. 10 (1991) 201.

[15] H.J. Borg, L.C.A. van den Oetelaar, L.J. van IJzendoorn and J.W. Niemantsverdriet, J. Vac. Sci. Technol. A 10 (1992) 2737.
[16] A.M. de Jong, H.J. Borg, L.J. van IJzendoorn, V.G.F.M. Soudant, V.H.J. de Beer, J.A.R. van Veen and J.W. Niemantsverdriet, J. Phys. Chem. 97 (1993) 6477.
[17] M. Bozoian, Nucl. Instr. and Meth. B 58 (1991) 127.
[18] T.W. Root, G.B. Fisher and L.D. Schmidt, J. Chem. Phys. 85 (1986) 4687.
[19] H.J. Borg, L.C.A. van den Oetelaar and J.W. Niemantsverdriet, Catal. Lett. 17 (1993) 81.
[20] R. Prins, V.H.J. de Beer and G.A. Somorjai, Cat. Rev. Sci. Eng. 31 (1989) 1.
[21] P. Mangnus, V.H.J. de Beer and J.A. Moulijn, Appl. Catal. 67 (1990) 119.
[22] J.C. Barbour, B.L. Doyle and S.M. Myers, Phys. Rev. B 38 (1988) 7005.
[23] N.A. North and C.A. Pearson, ICOM Committee for Conservation 4th meeting, 75/13/3/1-14, (1975).
[24] V.D. Daniels, L. Holland and M.W. Pascoe, Studies in Conservation 24 (1979) 85.
[25] S. Vepřek, J.Th. Elmer, Ch. Eckmann and M. Jurčik-Rajman, J. Electrochem. Soc. 134 (1987) 2398.
[26] M.J. de Graaf, R.J. Severens, M.J.F. van de Sande, M.C.M. van de Sanden and D.C. Schram, J. Nucl. Mat. 200 (1990) 380.
[27] F.H.P.M. Habraken, Nucl. Instr. and Meth. B 68 (1992) 181.
[28] L.J. van IJzendoorn, H.A. Rijken, S.S. Klein and M.J.A. de Voigt, Appl. Surf. Sci. 70/71 (1993) 58.
[29] H.A. Rijken, S.S. Klein, L.J. van IJzendoorn and M.J.A. de Voigt, Nucl. Instr. and Meth. B 79 (1993) 532.
[30] L.C. Feldman, J.W. Mayer and S.T. Picraux, Materials Analysis by Ion Channeling (Academic Press, 1982, New York).
[31] J.H. Barrett, Phys. Rev. B 3 (1971) 1527.
[32] J.H. Barrett, Nucl. Instr. and Meth. B 44 (1990) 367.